Drainage-induced spontaneous film climbing in capillaries

P. Pirdavari, H. Tran, Z. He, and M. Y. Pack*
Department of Mechanical Engineering, Baylor University, One Bear Place #97356, Waco, Texas 76798, USA

(Received 16 April 2024; accepted 27 August 2024; published 16 September 2024)

This study reports the ability with which surface tension gradients are formed plainly by the drainage in a capillary containing a surfactant-laden liquid slug initially held in place by a vacuum. Provided that a thin film forms on the walls transverse to the downward flow, the drainage induces a surfactant gradient (i.e., Marangoni effect), which then leads to a film-climbing event against gravity. The overall climbing effect is limited by the capillary rise height (i.e., propensity for infiltration due to surface tension) and the surfactant gradient formed postmeniscus drainage, thus revealing a twofold role of surface tension in gravity-oriented capillaries hitherto unexplored. The interplay of mechanisms influencing the climbing films include surfactant kinetics, diffusion, and advection of surfactants.

DOI: 10.1103/PhysRevFluids.9.094005

I. INTRODUCTION

The ability with which surface tension gradients cause an upswell or backflow against a wall is well documented in the presence of temperature gradients [1–4], surfactant generation by biofilms [5,6], pulmonary surfactant transport [7,8], and surfactant concentration gradients in a Landau-Levich (LL) [9–16] or Bretherton bubble (BB) [17–19] configuration. In each of these studies, surface tension gradient-induced flows, or Marangoni flows, may be classified by three modes [20]: thermal Marangoni [21–23], solutal Marangoni [24–26], and surfactant Marangoni flows [27–29], where the latter is the focus of this study. Although there are numerous studies harnessing Marangoni flows, their role in causing a backflow [30], or the film thickening effect in the context of BB [31] and LL [13] films has been controversial due to studies showing that instead of film thickening, film thinning is possible [17]. To understand how surfactants influence the thin-film dynamics, the overall competition among the relevant forces must be accounted for.

Previous studies have shown that three physical features govern the dynamics: surfactant kinetics (e.g., adsorption and desorption) [32], advection [33], and diffusion [34,35]. Bretherton first showed that the discrepancy between the pure lubrication theory prediction of the film thickness is shown for Capillary numbers below $\mathrm{Ca} < 5 \times 10^{-3}$. Ramdane and Quéré [9] balanced convection and adsorption in a diffusion-limited scenario of a wire-coating problem, where film thickening was attributed to Marangoni stresses. While the interplay of surfactant kinetics, advection, and diffusion generally represent the dominant interfacial transport dynamics, many studies have noted the potential influence of other physicochemical features on the film thickness such as the substrate roughness [36–38] or more broadly, slip effects [15,31]. Other effects on the film thickness include the influence of intermolecular forces [39,40], substrate charge, and surface impurities [41].

Recent works have shown the importance of thin-film formation in capillaries in the context of thermal management [42] and particle separations [43], yet it is not well understood how surfactants will affect the unsteady interfacial fluid dynamics inside capillaries. In this study, unsteady liquid films were generated by evacuating liquid slugs of various lengths in capillaries of different

*Contact author: min_pack@baylor.edu

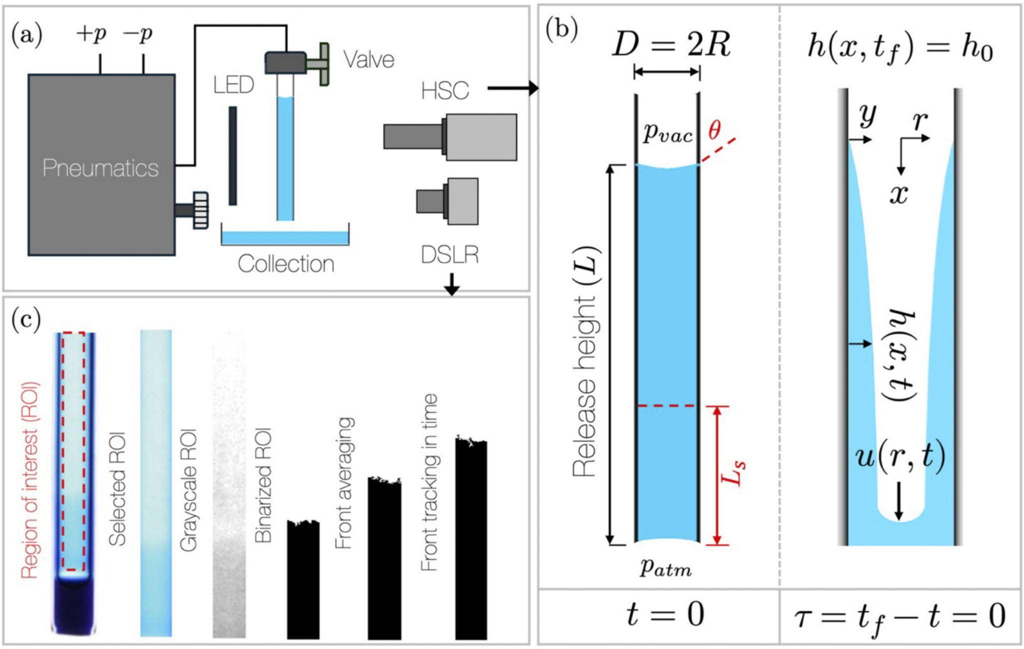

FIG. 1. A general overview of the experimental procedure. (a) Schematic of the experimental setup. HSC denotes high-speed camera and DSLR denotes digital single-lens reflex camera. LED denotes light-emitting diode and $+p$ and $-p$ denote the compressor and vacuum lines, respectively, for the pneumatics controller. (b) Schematic representation of the liquid slug before drainage and thin-film formation after the drainage. θ denotes the liquid-vapor (LV) contact angle, h is the thin-film thickness, h_0 the initial film thickness, D is the inner tube diameter, R is the inner tube radius, t_f the time it takes for the meniscus to reach the bottom of the tube, τ is the timescale related to the thin-film climbing, L_s denotes the static capillary rise height, u is the velocity in the x direction, and p_{vac} and p_{atm} denote the vacuum and the atmospheric pressures, respectively. (c) Steps involved in image processing of the film-climbing process.

diameters by gravitational drainage. Once the liquid slug drained, a residual thin film along the capillary wall allowed for surface tension gradients formed by surfactant concentration gradients at the liquid-air interface allowing the spontaneous motion upwards. The theoretical modeling efforts and the critical timescales for the film-climbing event were explored in this study accounting for advection, diffusion, and adsorption/desorption dynamics at the liquid-air interface.

II. METHODS

A. Experimental methods

A schematic illustration of the experimental setup is shown in Fig. 1(a). A pneumatic pressure controller was utilized to regulate the vacuum pressure inside the tube and to facilitate the suction of the solution from the collection Petri dish, enabling the liquid slug to reach the initial release height, L. Following the completion of the suction process, the laboratory jack supporting the Petri dish was lowered, thereby severing the connection between the liquid slug within the tube and the liquid pool in the Petri dish. During the experiment, a valve was used to release the vacuum pressure and initiate the downward flow of the liquid. Due to the fast dynamics of this problem, the falling meniscus of the liquid slug was monitored by a high-speed camera (HSC; Vision Research, Phantom V211) with a frame rate of 5000 frames per second (fps). The velocity of the meniscus was then tracked using a custom-built matlab code. For capturing and analyzing the dynamics of the climbing film induced by the Marangoni stress, a digital single-lens reflex (DSLR) camera was operated at a frame rate of 30 fps, and the backlight was provided by a light-emitting diode (LED) panel. To mitigate dewetting on the tube surface, glass tubes were cleaned by 15-min ultrasonication in the following sequence: detergent solution (Sparkleen, Fisher Scientific), ethanol, acetone, and deionized (DI) water, and subsequently dried with compressed air. After ultrasonication with the detergent solution, the tubes were rinsed with DI water before undergoing subsequent ultrasonication steps with ethanol and acetone. The tubes were cleaned after each experimental trial to limit contamination from the environment. As shown in Fig. 1(b), prior to drainage, the liquid slug was held at L briefly prior to opening the valve to release the slug. Upon drainage ($t = 0$), the meniscus fell rapidly and due to the wetting tube walls, a thin film was left behind on the walls. τ represents the relevant timescale for the Marangoni stress-induced climbing film, where $\tau = 0$ corresponds to the moment the falling meniscus reaches the bottom of the tube ($t = t_f$). To capture the climbing film front, a custom-built matlab code was used. Figure 1(c) shows the climbing film tracking procedure we used in the image analysis. First, a region of interest was selected for analysis and converted into grayscale. Then, the images were binarized using adaptive thresholding which enabled the distinction of the climbing film by setting pixels below a certain intensity level to black (background) and those above are set to white (climbing film). Furthermore, the noise, which may be caused by various factors such as fluctuations in the lighting, was removed by eliminating connected components in the binary image that have fewer than a specified number of pixels. Finally, the data for the climbing front position was smoothed by local regression using weighted linear least squares and a second degree polynomial model. This process was repeated for all frames, resulting in the time series of the climbing film front position.

B. Sample preparation

To enhance the image contrast of the liquid, methylene blue (MB; Sigma-Aldrich) at a concentration of 0.1 wt. %, was dissolved in type 1 deionized water (18.2 MΩ cm; Synergy, MilliporeSigma). Sodium dodecyl sulfate (SDS; MilliporeSigma) was then added to the MB-water solutions. The bulk concentration of SDS, denoted as C, varied between 0.1 and 7 mM.

C. Interferometry

To extract the film thickness (h) during the drainage within the tube, we directly measured the thin-film thickness within the tube using interferometry. Since the thin films within the tube are much smaller than the tube radii, we also compared the drainage to glass slides. We thus describe two different procedures for obtaining thin films on a glass tube and glass slide.

Glass slide. A cleaned and plasma-treated glass slide was positioned vertically and the solution was injected on its surface such that the whole width of the glass slide was wetted. Upon cessation of the injection, the high-speed camera captured the video recording to capture the interference patterns.

Glass tube. The solution was suctioned to the prescribed height inside a cleaned tube. In order to diminish the curvature effect of the tube, two cleaned glass slides were attached on the opposite sides of the tube using clear epoxy. The draining film region was illuminated by a 22.5 mW He-Ne laser (632.8 nm; ThorLabs), and the interference patterns were recorded by the HSC with a frame rate of 100 fps. At a given fixed region of interest far from the contact line, the fringes were counted by analyzing the interference patterns between successive frames. Peaks in the intensity profile were detected to identify the interference fringes. Using these detected peaks, the total number of fringes (N_f) was counted from the start of the drainage until the contact line passed through the region of interest, which occurs at late times due to dewetting. The total film thickness is then $h = N_f \lambda/(2n)$ where λ is the laser wavelength and n is the refractive index of the solution. Therefore, the changes in N_f in time provide the temporal changes in the film thickness at the region of interest.

D. Fluid statics prior to drainage

The initial condition of the experiments consists of a liquid slug held with vacuum pressure, $p_{\rm vac}$, defined as [refer to Fig. 1(b)]

$$p_{\rm vac} = p_{\rm atm} - \rho g \mathcal{B}, \tag{1}$$

where $p_{\rm atm}$ is the atmospheric pressure and $\mathcal{B} = L - L_s$. L_s is the static capillary rise height given by

$$L_s = \frac{4\ell_c^2 \cos\theta}{D}, \tag{2}$$

where $\ell_c = \sqrt{\gamma/(\rho g)}$ is the capillary length, γ the surface tension, θ the LV contact angle (measured from the solid to the liquid-vapor interface), $D = 2R$ the tube diameter, and R the tube radius. The LV surface area, SA, sets the potential for surface tension gradients and is given by

$$\mathrm{SA} = 2\pi R^2 \left(\frac{1 - \sin\theta}{1 - \sin^2\theta}\right). \tag{3}$$

At the limit of perfect wetting, $\mathrm{SA} = 2\pi R^2$, $\theta = 0^\circ$ and at the limit of no wetting $\theta \to 90^\circ$, $\mathrm{SA} = \pi R^2$ and $L_s = 0$. We presume that prior to the drainage of the slug, the bulk $C < C_m$ (M/m^3) and surface $\Gamma < \Gamma_m$ (M/m^2) concentrations of surfactant are less than the critical micelle concentration (subscript m) as soluble surfactants adsorb and desorb from the liquid-vapor interface. Above C_m, micelles begin to form, yet without a further decrease in the surface tension. We thus assume that the wettability of the tubes sets the initial amount of moles, n_s, at the time $t = 0$ s (i.e., right before the drainage of the liquid slug), of the surfactants on the LV interface, $n_s(t) = n_s(0) = [\mathrm{SA}(0)]\Gamma$. The equilibrium surface to bulk concentrations denoted by $\Gamma_{\rm eq}$ and C, respectively, will set the length scale [11,44], $\ell_D = \Gamma_{\rm eq}/C$, and $\Gamma_{\rm eq}$ may be approximated by the Gibbs isotherm,

$$\Gamma_{\rm eq} = -\frac{1}{\mathcal{R}T}\frac{d\gamma}{d(\ln C)}, \tag{4}$$

with $\mathcal{R}$ the universal gas constant and T the temperature.

E. The governing timescales in the dynamics

Four competing effects presumably influence the dynamics as a draining liquid slug leaves behind a film along the tube wall: (i) diffusion, (ii) adsorption, (iii) desorption, and (iv) advection.

Diffusion. Assuming that the surface diffusivity of SDS, $\mathcal{D}_s$, is comparable to the bulk diffusivity $\mathcal{D}$, and also presuming that the length scale for the bulk diffusion is much smaller than the surface diffusion [45], the bulk diffusion dominates the diffusion dynamics relative to the surface diffusion, and the relevant length scale for diffusion from the bulk to the interface is ℓ_D as described above. The ability with which the surfactants reach the liquid-air interface during the drainage of the slug will determine whether the climbing film may form, and the overall diffusion timescale is then $t_D = \ell_D^2/\mathcal{D}$.

Advection. Irrespective of the capillary size, the meniscus shape is related to the capillary length and thus ℓ_c sets the interfacial length scale, and the advection timescale is given by $t_C = \ell_c/\overline{V}$, where $\overline{V}$ is the average velocity within the draining liquid slug. Therefore, at the interface, the Peclet number, $\mathrm{Pe} = t_D/t_C = \overline{V}\ell_D^2/(\mathcal{D}\ell_c) = \mathcal{O}(10^{-2} - 10^0)$, for SDS concentrations between 1 and 7 mM, where the dynamics are advection dominant at lower surfactant concentrations and diffusion dominant at higher concentrations. We expect that if surface diffusion was important, then Pe becomes $\mathrm{Pe}_s = \overline{V}\ell_c/\mathcal{D}_s$, which would always make the dynamics advection dominant. Once a thin film forms from the drainage of the liquid slug, the propensity for the climbing film to manifest will be set by the Marangoni number, $\mathrm{Ma}_s = (d\gamma/dC)\Delta CL/(\mu D_s)$. Since $\mathrm{Ma}_s \gg 1$ for all experiments, it guarantees an upward climbing film provided a surfactant gradient exists along the liquid-air interface.

Surfactant kinetics. The adsorption timescale refers to the net adsorption in the surfactant kinetics encompassing both the adsorption, $t_a = \Gamma_m/(k_a C)$, and the desorption, $t_d = 1/k_d$, timescales, where k_a and k_d are the adsorption and desorption coefficients, respectively, with the surfactants obeying Langmuirian kinetics [46]. $k_a = 6.4 \times 10^{-6}$ m/s and $k_d = 5.8$ 1/s, which were previously reported for SDS [36]. Note that we defined $k_a = \beta\Gamma_m$, where β is the adsorption rate constant [46] (sometimes used as k_a in the literature [47,48]). Several other dimensionless groups related to the surfactant kinetics arise including the Damkohler, $\mathrm{Da} = \Gamma_m/(\ell_c C)$, Biot, $\mathrm{Bi} = k_d \ell_c/\overline{V}$, and the Langmuir, $\mathrm{La} = k_a C/(k_d \Gamma_m)$ numbers. The Da relates the diffusion time to the kinetic timescales (e.g., reaction-diffusion problems), Bi defines the relative importance of the interfacial surfactant exchange rate to the interface velocity, and La measures the rate of interfacial adsorption to the rate of desorption driven by entropic effects at the interface [46–49]. In this study, $\mathrm{Da} = \mathcal{O}(10^{-2} - 10^{-1})$ and $\mathrm{Bi} = \mathcal{O}(10^{-3} - 10^{-2})$ and thus the surfactant diffusion and advection dominate the surfactant kinetic effects. Interestingly, the $\mathrm{La} = \mathcal{O}(10^{-2} - 10^{0})$ between 0.1 and 7 mM SDS concentrations, which shows the relative importance of adsorption over desorption at higher surfactant concentrations, which may potentially cause a reduction in the surfactant gradients along the thin film due to the surfactant accumulation at the interface, albeit to a small degree relative to diffusion and advection. At low SDS concentrations, we hypothesize that the drainage is advection dominant and thus Marangoni flows should be present. As the surfactant concentration is increased in the solution, the ℓ_D becomes smaller [50], which results in smaller diffusion and adsorption timescales while the desorption timescale stays constant. We thus hypothesize that at higher surfactant concentrations, the faster diffusion cancels out any surface tension gradients induced by advection, which would prevent the climbing film from occurring.

III. RESULTS

A. Drainage of the liquid slug

Figure 2(a) shows the pre- and postdrainage images of 2 and 7.75 mm tubes for $L = 4$ cm. For both cases, a small liquid slug remains at the tip of the tube after the drainage. As the tube diameter is increased beyond a critical tube diameter (10–15 mm for water), no liquid is retained inside the tube post drainage [51]. For smaller tube diameters, capillary forces help retain a taller residual slug.

We now seek to describe the drainage dynamics of the liquid slug. Assuming one-dimensional flow approximation and that the control volume (CV) envelops the liquid slug and accelerates with it (e.g., noninertial reference frame), the linear momentum by the Reynolds transport theorem provides [52]

$$\sum F - \int_{\mathcal{V}} \rho a_{\mathrm{rel}} d\mathcal{V} = \frac{d}{dt}\int_{\mathcal{V}} \rho \underline{V} d\mathcal{V} + \int_{\mathcal{A}} \rho \underline{V}(\underline{V} \cdot \hat{n}) d\mathcal{A}, \tag{5}$$

where $\mathcal{V}$ and $\mathcal{A}$ denote the volume and area integrals, respectively, $\underline{V}$ is the velocity, and $\hat{n}$ is the unit normal vector. $\sum F$ represents the sum of all of the surface and body forces and $\int_{\mathcal{V}} \rho a_{\mathrm{rel}} d\mathcal{V}$ is a consequence of the acceleration of the CV with respect to an inertial reference frame. In Eq. (5), the right-hand side of the equation represents motion with respect to an accelerating coordinate system and thus the rate of change of momentum inside the accelerating CV and the net momentum flux through the control surface are both zero.

By assuming that the gravity, the pressure forces, and the viscous forces are the governing forces acting on the liquid slug, $\sum F$ can be written as $\rho\mathcal{V}g + \Delta p A - \sigma A_w$, where the first term is the gravitational force, the second term is the pressure force (e.g., capillary force), and the third term is the viscous resistance. We note that $A = \pi R^2$ is the cross-sectional area of the tube whereas $A_w = 2\pi R L$ is the wetted area of the tube wall. σ denotes the shear stress within the tube. Thus, Eq. (5) may be written as

$$\rho\mathcal{V}g + \Delta p A - \sigma A_w - \rho\mathcal{V}a_{\mathrm{rel}} = 0. \tag{6}$$

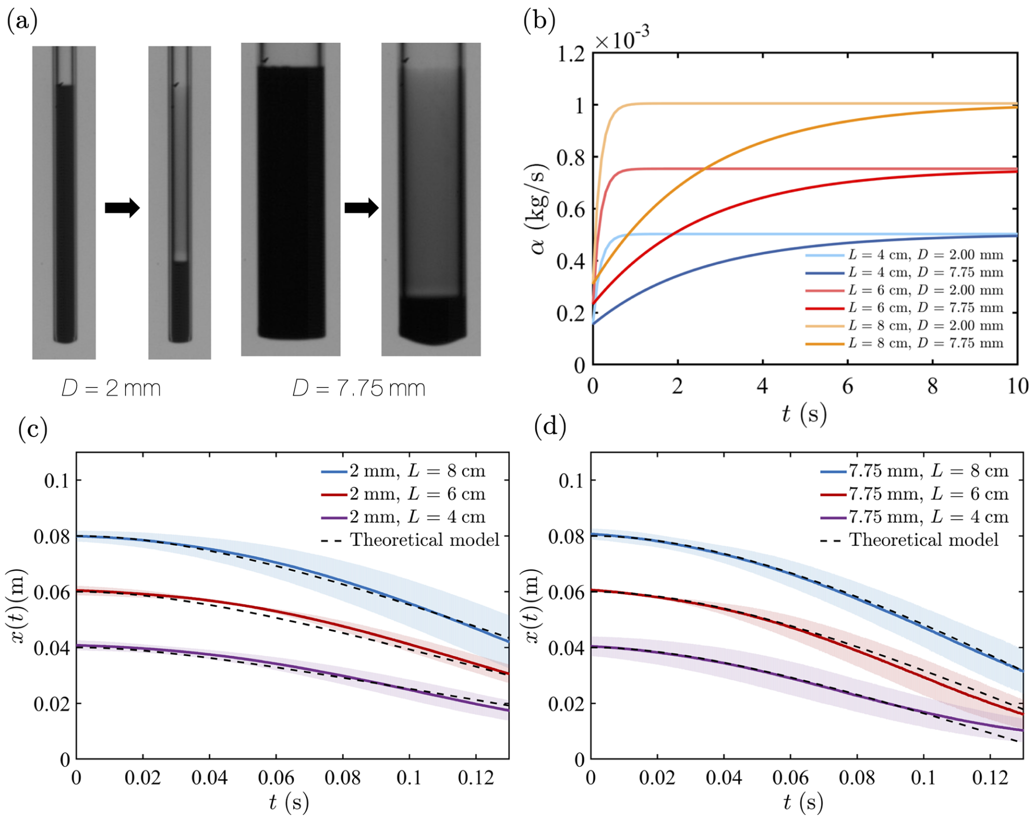

FIG. 2. Dynamics of the falling meniscus. (a) Meniscus position before and after the drainage for $L = 4$ cm with $D = 2$ mm and $D = 7$ mm. The residual thin film on the wetting walls is shown above the residual meniscus post drainage with minimal dewetting. (b) Temporal variations of α for different release heights and tube diameters. (c) Temporal variations in the falling meniscus position at different release heights for $D = 2$ mm and (d) $D = 7.75$ mm. The dashed lines represent Eq. (16) and the error bars represent the standard deviation of three experiments.

The shear stress, σ, may be obtained from $\sigma = \mu \frac{\partial V}{\partial r}$ where $\frac{\partial V}{\partial r}$ is the velocity gradient perpendicular to the flow. Therefore, the viscous force is

$$F_v = \sigma A_w = \mu \frac{\partial V(r,t)}{\partial r}(2\pi RL). \tag{7}$$

For fully developed flow, the shear stress in the tube may be expressed as $\sigma = 2\mu V_{\max}/R$ where $V_{\max}$ is the maximum velocity, which occurs at the tube center. Thus, the viscous resistance for the fully developed cases is given by $F_v = 4\mu\pi L V_{\max}$. However, for such short tubes utilized in our study and at larger tube diameters, the fully developed flow assumption during drainage is invalid. We thus considered the transient dynamics of the viscous losses and have derived the factor $\alpha(t)$ where it is related to the instantaneous viscous force as

$$F_v = \mu \frac{\partial V(r,t)}{\partial r}(2\pi RL) = \alpha(t) V_{\max}. \tag{8}$$

To obtain $\alpha(t)$, we consider the unidirectional unsteady pipe flow equation:

$$\rho \frac{\partial V}{\partial t} = -\frac{dp}{dz} + \mu\left(\frac{\partial^2 V}{\partial r^2} + \frac{1}{r}\frac{\partial V}{\partial r}\right). \tag{9}$$

$\frac{dp}{dz}$ is the pressure gradient of the draining liquid slug in the direction of the drainage. Given the initial condition of $V(r,0)=0$ and the no-slip boundary condition at the tube wall, $V(R,t)=0$, and by nondimensionalizing the equation using

$$\tilde{t}=\frac{\mu t}{\rho R^2},\quad \tilde{r}=\frac{r}{R},\quad \tilde{V}=\frac{V}{V_{\max}}, \tag{10}$$

where $\tilde{V}$, $\tilde{r}$, and $\tilde{t}$ are the dimensionless velocity, radius, and time, respectively,

$$\frac{\partial\tilde{V}}{\partial\tilde{t}}=\frac{1}{\tilde{r}}\frac{\partial}{\partial\tilde{r}}\left(\tilde{r}\frac{\partial\tilde{V}}{\partial\tilde{r}}\right). \tag{11}$$

Separation of the variables results in

$$\frac{V(r,t)}{V_{\max}}=1-\left(\frac{r}{R}\right)^2-8\sum_{n=1}^{\infty}\frac{J_0\left(\lambda_n\frac{r}{R}\right)}{\lambda_n^3J_1(\lambda_n)}\exp\left[\frac{-\mu\lambda_1^2t}{\rho R^2}\right], \tag{12}$$

where $J_1(\lambda_1)$ is the Bessel function of the first kind of order 1; λ_1 refers to the first positive root of $J_1(\lambda_1)=0$. By taking the derivative of Eq. (12) and substituting it in Eq. (8), α is obtained as

$$\alpha=2\pi RL\mu\left(-\frac{2r}{R^2}+\frac{8}{R}\frac{J_1\left(\lambda_1\frac{r}{R}\right)}{\lambda_1^2J_1(\lambda_1)}\exp\left[\frac{-\mu\lambda_1^2t}{\rho R^2}\right]\right). \tag{13}$$

Temporal variations of α are shown in Fig. 2(b) for two tube diameters and three release heights. The value of α increases over time and eventually converges to the fully developed value, $\alpha_{FD}=4\pi L\mu$, for all cases. The α_{FD} values for $L=4$, 6, and 8 cm, are 5.02×10^{-4}, 7.54×10^{-4}, and 10^{-3} kg/s, respectively. For the $D=2$ mm tube, the fully developed assumption is reasonable. However, for $D=7.75$ mm, it takes longer for α to reach the fully developed value. We average α over time to obtain the average contribution of the transient viscous losses at the tube wall where the average value is then

$$\bar{\alpha}=\frac{1}{t_f}\int_0^{t_f}\alpha\,dt=\frac{-2\pi RL\mu}{t_f}\left[\frac{2}{R}t_f+\frac{8\rho R}{\mu\lambda_1^4}\exp\left(\frac{-\mu\lambda_1^2t_f}{\rho R^2}\right)\right]. \tag{14}$$

The meniscus falling velocity, $V(t)$, may be obtained by solving the transport equation (6) by an integrating factor and given as

$$V(t)=\frac{\pi\rho gR^2L}{\bar{\alpha}}\left(1-\frac{L_s}{L}\right)\left[1-\exp\left(-\frac{\bar{\alpha}t}{\pi\rho R^2L}\right)\right]. \tag{15}$$

Integrating Eq. (15) in time provides the meniscus position, $x(t)$, given by

$$x(t)=\frac{\zeta}{\varepsilon}\left[\frac{1}{\varepsilon}\exp(-\varepsilon t)+t-\frac{1}{\varepsilon}\right]+L, \tag{16}$$

where $\zeta=g(1-L_s/L)$ and $\varepsilon=\bar{\alpha}/(\pi\rho^2L)$. To validate the drainage problem and the theoretical model, the position of the meniscus was tracked during drainage at three release heights ($L=4$, 6, and 8 cm) inside two tubes with diameters of 2 and 7.75 mm using a HSC. Variations of the meniscus position with time were obtained using a custom-built matlab code. The data averaged from three experiments for each release height is shown along with error bars depicting the standard deviation of the results and compared with the theoretical model in Figs. 2(c) and 2(d) for $D=2$ and 7.75 mm. The experimental results have good agreement with the theoretical model. In the initial stages, the majority of cases exhibit small error bars. However, the increasing error bars over time may be attributed to dewetting on the tube walls giving less certainty in the measurements over time. Increasing the tube diameter from 2 to 7.75 mm resulted in a faster drainage of the liquid, which was due to the increased inertia of the liquid slug in the larger tube diameter.

B. Post drainage of the liquid slug: The drainage of the thin liquid film

If the tube walls are wetting, the meniscus falls rapidly such that a thin film is left behind on the walls. The viscous, gravity-driven thin-film drainage at steady state turns into

$$\frac{d^2u}{dy^2} = \frac{\rho g}{\mu}, \tag{17}$$

where $u(y)$ is the velocity of the draining film. y is the direction perpendicular to the surface and μ is the dynamic viscosity of the liquid. By taking the no-slip boundary condition at the surface ($y = 0$) and zero shear at the film-air interface ($y = h$) into account, the Navier-Stokes (NS) equation may be simplified as

$$u(y) = \frac{\rho g}{2\mu}(2hy - y^2). \tag{18}$$

Thus, the average draining film velocity, $\overline{u_f}$, is calculated as

$$\overline{u_f} = \frac{1}{h}\int_0^h u(y)dy = \frac{\rho g h^2}{3\mu}. \tag{19}$$

Since the film thickness changes over time slowly, the quasistatic film thickness is found by setting a similarity variable, $\eta = z(2\nu/g)^{-1/2}(x/t)^{-1/2}$, where ν is the kinematic viscosity of the film to solve

$$\frac{\partial h}{\partial t} = \frac{-gh^2}{\nu}\frac{\partial h}{\partial x}. \tag{20}$$

The following relationship was obtained previously by Jeffreys [53]:

$$h = \sqrt{\frac{\mu x}{\rho g t}}. \tag{21}$$

If the film thickness, h, was $h \sim \mathcal{O}(100\ \mu\text{m})$, the drainage timescale, $t_{\text{drain}} = 3L\nu/(gh_0^2) \sim \mathcal{O}(1\ \text{s})$, where we recall that h_0 is the initial film thickness and thus drainage of the thin film is indeed much slower than the meniscus falling velocity.

Once a thin film is formed on the walls post-meniscus drop, the existence of surface tension gradients ($\frac{d\gamma}{dx}$) will create Marangoni stress along the thin film. Thus, at the liquid-air interface ($y = h$), $\mu\frac{du}{dy} = \frac{d\gamma}{dx} = \frac{d\gamma}{dC}\frac{\partial C}{\partial x}$ and there is no slip on the wall [$u(y = 0) = 0$)] By solving the NS equation for thin-film drainage [i.e., Eq. (17)] and applying these boundary conditions, the velocity profile within the thin film will be governed by

$$u(h) = \frac{g}{2\nu}h^2 + \frac{h}{\mu}\frac{d\gamma}{dC}\frac{\partial C}{\partial x}. \tag{22}$$

We suspect that the Marangoni and the gravitational drainage velocities should scale as $u_M \sim \frac{h_0}{\mu}\frac{d\gamma}{dC}\frac{\partial C}{\partial x}$ and $u_G \sim \frac{g}{2\nu}h^2$, respectively.

For the drainage of the thin liquid film in a tube, we solved the NS equation for gravity-driven drainage in cylindrical coordinates considering a no-slip condition at the tube wall ($r = R$), and zero shear at the film-air interface ($r = R - h$); the velocity at the film-air interface was obtained as

$$u(R - h) = \frac{\rho g}{4\mu}\left[2Rh - h^2 + 2(R - h)^2 \ln\frac{R - h}{R}\right]. \tag{23}$$

By solving this equation implicitly for h, and letting $u = x/t$, an approximation was obtained for the temporal variations of the film thickness during the film drainage. In Fig. 5, the initial thin-film drainage height was similar across all cases involving both the flat plate and the cylindrical geometries and across all surfactant concentrations. We note that the cylindrical case initially overestimated the film thickness; however, it aligned well with the tube interferometry results

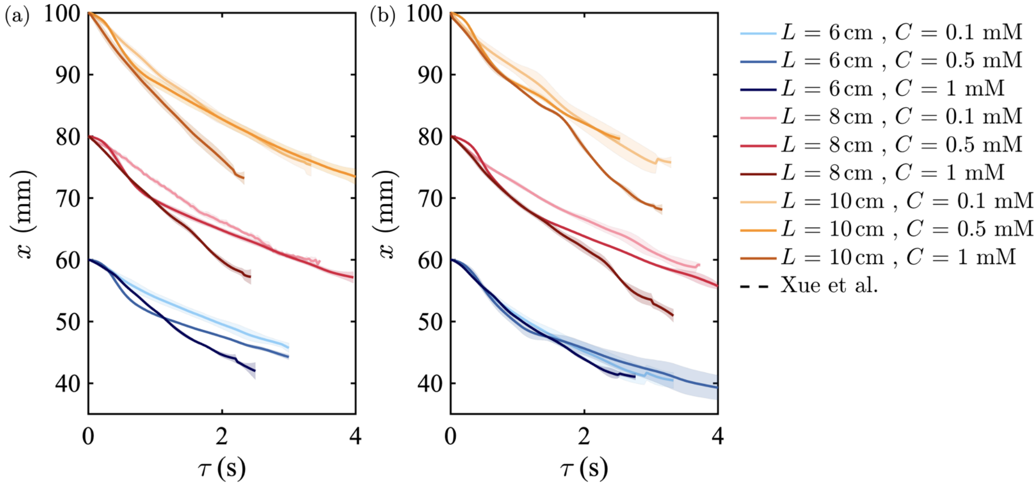

FIG. 3. Temporal variations of climbing film front position. (a) $D = 3.9$ mm; (b) $D = 7.75$ mm. Sudden changes in the slope in (b) are caused by dripping from the tube, where the recoil enhances the climbing effect.

at intermediate times. At late times, the thin-film dewetting caused stronger deviations from the theoretical models.

Three solutions of MB containing various SDS concentrations (0.1, 0.5, and 1 mM) below the C_m were drained from tubes with diameters of 3.9 and 7.75 mm. The release occurred at different heights ($L = 6$, 8, and 10 cm). Following the drainage of the liquid slug, a climbing film emerged from the top of the meniscus at the bottom of the tube, where the motion was induced by the surface tension gradient resulting from the drainage of the SDS solution. Temporal variations of the climbing front position for all studied cases are shown in Fig. 3. The experiments were conducted three times, and the averaged results, accompanied by their corresponding error bars, are presented. $x = 0$ is the release position of the initial liquid slug prior to release. Thus, depending on the release height of the liquid slug, $x(t = 0)$ varies for different cases. We found that the initial surfactant concentration had a weak effect on the climbing rate although at 1 mM ($D = 3.9$ mm), the climbing rate was faster. We attribute this to the higher surfactant aggregation at the liquid-air interface causing a stronger Marangoni stress. For cases with higher release heights ($D = 7.75$ mm), sudden acceleration of the climbing film was observed for the 1 mM surfactant concentration at 6 and 8 cm [Fig. 3(b)], which was attributed to drop pinch-off at the tip of the tubes. The pinch-off events causes the climbing film to recoil and accelerate.

IV. DISCUSSION

Based on our hypothesis, advection must dominate diffusion and surfactant kinetics for film climbing. To validate our hypothesis, experiments were also conducted for two higher SDS concentrations (3 and 7 mM) at three release heights (6, 8, and 10 cm). The schematic and experimental representation of the postigdrainage dynamics is shown in Fig. 4 for the drainage of 1, 3, and 7 mM SDS solutions inside a $D = 7.75$ mm tube for the release height of $L = 10$ cm. A clear climbing film post drainage can be observed for $C = 1$ mm as seen in Fig. 4(a). For $C = 3$ mm, the drainage film forms on the tube walls, but no climbing film is observed. For this case, diffusion, adsorption, desorption, and advection timescales are calculated as 2×10^{-3}, 0.46, 0.17, and 7×10^{-3} s. It is evident that the diffusion timescale is considerably smaller than the advection, which shows that the problem is not advection dominant anymore. This observation proves our hypothesis that at higher SDS concentrations, diffusion gains more dominance and eventually diminishes the surfactant gradients caused by advection as the result of gravitational drainage. For 7 mM, it was observed

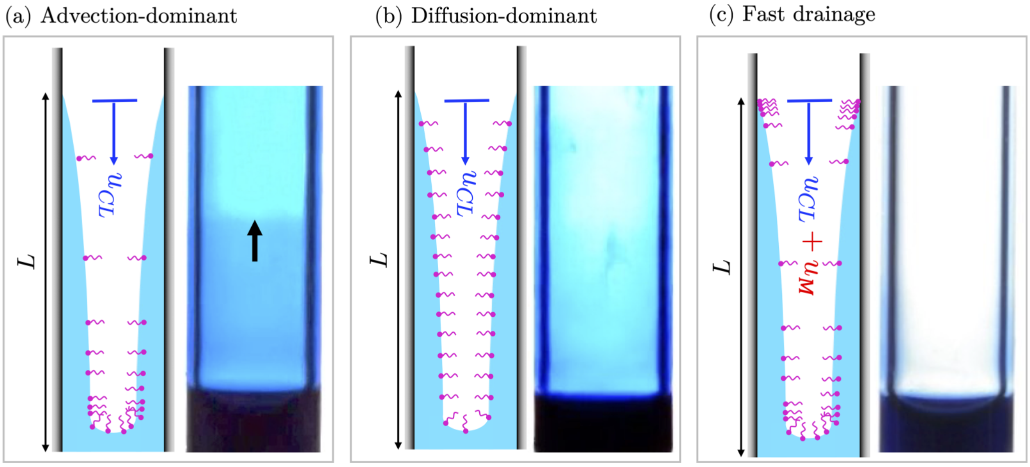

FIG. 4. Schematic and experimental representation of postdrainage dynamics: (a) advection-dominant ($C = 1$ mM) case where the strong flow creates axial surfactant gradients at low surfactant concentrations; (b) diffusion-dominant ($C = 3$ mM) case where the dominant diffusion of surfactants to the liquid-air interface prevents surfactant gradients at intermediate surfactant concentrations; and (c) fast drainage ($C = 7$ mM) case where we postulate that surfactants at the contact line cause a surfactant gradient to enhance drainage of the thin film at the highest surfactant concentrations. u_{CL} is the contact line velocity due to dewetting and u_M is the Marangoni velocity.

that the high SDS concentrations caused dewetting on the tube walls hindering the formation of the thin films upon drainage as seen in Fig. 4(c) (see Supplemental Material [54] and compare the 1 mM case with the 7 mM case). We suggest that near the precursor film in the contact line of the draining film, surfactants are densely packed at the highest surfactant case, where such effect is not as strong at lower surfactant concentrations. Therefore, once the liquid slug is drained for the 7 mM case, the Marangoni effect acts in the direction of the drainage causing stronger dewetting. We thus show that increasing the SDS concentration beyond a critical threshold (≈ 3 mM) not only fails to yield the climbing film but also hinders the formation of thin wetting films in general.

If a climbing film forms, we may describe the climbing dynamics in the following way by adopting the same assumptions as Xue *et al.* [16] except that we have set the origin at the release height of the liquid slug as opposed to setting the origin at the start of the climbing film. The key difference between the Xue *et al.* study and the current study lies in the fact that in the present study, the Marangoni stress is purely due to drainage and not due to a sudden change in the surfactant concentration between the pure thin liquid film and a surfactant bath. From Eq. (22), the velocity ratio of Marangoni, u_M, to the gravitational drainage, u_G, is given as $\Lambda_f = \frac{d\gamma}{dC}\frac{2}{\rho g h}\frac{\partial C}{\partial x}$. Considering $\frac{\partial C}{\partial x} \sim \frac{C}{L}$, Λ_f is estimated as

$$\Lambda_f = \frac{d\gamma}{dC}\frac{2C}{\rho g h L}. \tag{24}$$

By substituting the film thickness from Jeffreys' solution for film thickness [53] ($h = \sqrt{\frac{\mu x}{\rho g \tau}}$), the velocity ratio is obtained as

$$\Lambda_{fc} = \frac{d\gamma}{dC}\frac{2C}{\rho g L}\left[\frac{\rho g \tau}{\mu x}\right]^{1/2}. \tag{25}$$

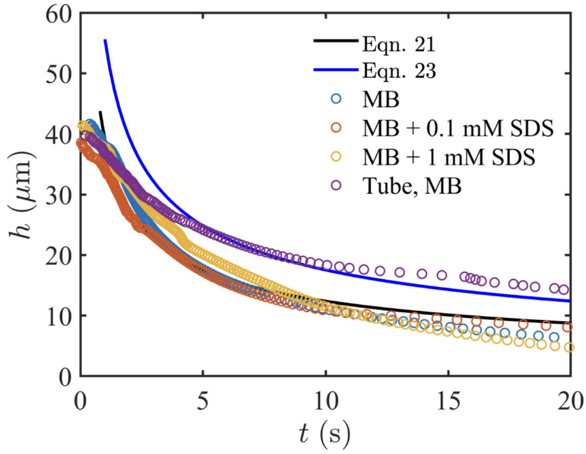

FIG. 5. Temporal variation of the draining film thickness across various MB and SDS surfactant concentrations. The black line is the Jeffreys solution [Eq. (21)] and the blue line is Eq. (23).

By setting $x = L$, the climbing film timescale (τ_d) is calculated by

$$\tau_d = \frac{\Lambda_{fc}^2 \mu \rho g L^3}{4\left(C\frac{d\gamma}{dC}\right)^2}. \tag{26}$$

The dimensionless climbing film front position ($\tilde{x}$) and time ($\tilde{\tau}$) are obtained as $\tilde{x} = x/L$ and $\tilde{\tau} = \tau/\tau_d$, respectively, where x is the climbing film front position. The expected Marangoni upward climbing rate is given by

$$\tilde{x} = 1 - \tilde{\tau}^{2/3}. \tag{27}$$

In order to obtain the value of $\tilde{\tau}$, an estimation of the film thickness (h) was obtained from Fig. 5. The experimentally derived h was also used to calculate λ_f and τ_d for each case. In order to compare the experiments with the model ($\tilde{x} = 1 - \tilde{\tau}^{2/3}$), the climbing film time (τ) and position (x) were nondimensionalized using L and τ_d, respectively. The nondimensional results for all SDS concentrations and release heights are portrayed in Fig. 6 along with the model. $\tilde{x} = 1$ refers to the tip of the tube where the climbing film starts and $\tilde{x} = 0$ signifies the release height of the liquid slug. After nondimensionalizing the data, there was a notable collapse across different concentrations and release heights, showing good agreement with the theoretical model particularly at early times (i.e., before drop pinch-off events).

V. CONCLUSIONS

Surfactant-laden liquid slug drainage and the subsequent spontaneous film climbing was investigated inside circular capillary tubes. We found that the draining film imparts a surface tension gradient that results in a climbing film. Different tube diameters, liquid slug release heights, and surfactant concentrations were studied. The key findings are as follows:

(1) Decreasing the capillarity diameter resulted in a deceleration of the liquid slug drainage due to the increased capillary and viscous resistance.

(2) At low surfactant concentrations, advection was dominant, which enabled the formation of climbing films caused by surfactant gradients.

(3) At higher surfactant concentrations, diffusion overcame advection and suppressed the surfactant gradients.

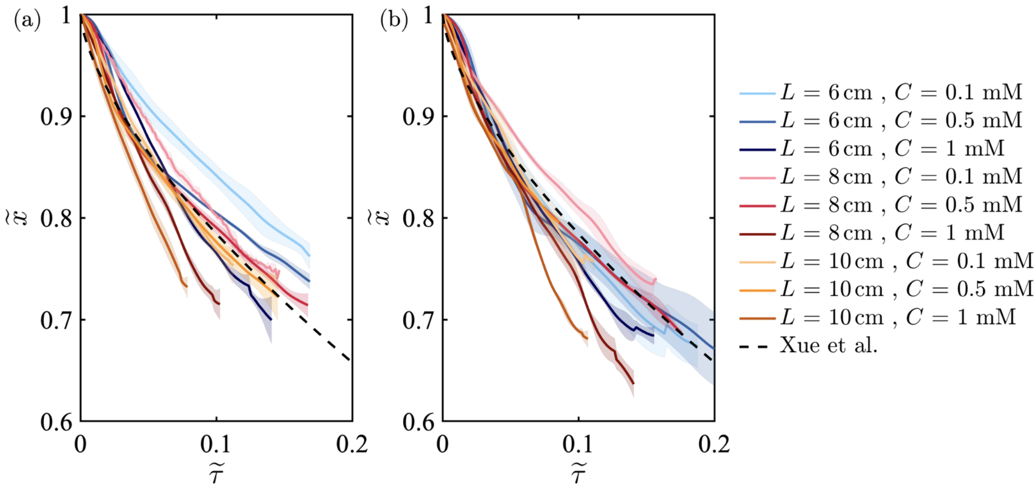

FIG. 6. Dimensionless temporal variations of the climbing film front position and comparison with the model [Eq. (27)] for (a) $D = 3.9$ mm and (b) $D = 7.75$ mm. The surfactant variation was between 0.1and 1 mM across liquid slug release heights between 6 and 10 cm.

(4) At the highest surfactant concentrations close to the critical micelle concentration, there was no residual thin film or a climbing film and instead, instant dewetting as the liquid slug drained was observed.

ACKNOWLEDGMENT

The authors thank Baylor University's startup funds for the support of this work.

[1] V. Ludviksson and E. Lightfoot, The dynamics of thin liquid films in the presence of surface-tension gradients, AIChE J. **17**, 1166 (1971).

[2] A. Cazabat, F. Heslot, S. Troian, and P. Carles, Fingering instability of thin spreading films driven by temperature gradients, Nature (London) **346**, 824 (1990).

[3] X. Fanton, A. Cazabat, and D. Quéré, Thickness and shape of films driven by a Marangoni flow, Langmuir **12**, 5875 (1996).

[4] D. Kang, A. Nadim, and M. Chugunova, Marangoni effects on a thin liquid film coating a sphere with axial or radial thermal gradients, Phys. Fluids **29**, 072106 (2017).

[5] T. E. Angelini, M. Roper, R. Kolter, D. A. Weitz, and M. P. Brenner, *Bacillus subtilis* spreads by surfing on waves of surfactant, Proc. Natl. Acad. Sci. USA **106**, 18109 (2009).

[6] P. K. Jha, H. Dallagi, E. Richard, T. Benezech, and C. Faille, Formation and resistance to cleaning of biofilms at air-liquid-wall interface. Influence of bacterial strain and material, Food Control **118**, 107384 (2020).

[7] J. B. Grotberg, Pulmonary flow and transport phenomena, Annu. Rev. Fluid Mech. **26**, 529 (1994).

[8] D. Kang, M. Chugunova, A. Nadim, A. Waring, and F. Walther, Modeling coating flow and surfactant dynamics inside the alveolar compartment, J. Eng. Math. **113**, 23 (2018).

[9] O. Ou Ramdane and D. Quéré, Thickening factor in Marangoni coating, Langmuir **13**, 2911 (1997).

[10] A. Münch and P. Evans, Marangoni-driven liquid films rising out of a meniscus onto a nearly-horizontal substrate, Physica D (Amsterdam, Neth.) **209**, 164 (2005).

[11] R. Krechetnikov and G. M. Homsy, Surfactant effects in the Landau–Levich problem, J. Fluid Mech. **559**, 429 (2006).

[12] E. Ramé, The stagnation point in Marangoni-thickened Landau-Levich type flows, Phys. Fluids **19**, 078102 (2007).

[13] H. Mayer and R. Krechetnikov, Landau-Levich flow visualization: Revealing the flow topology responsible for the film thickening phenomena, Phys. Fluids **24**, 052103 (2012).

[14] S. Gupta and N. Tiwari, Dip coating in the presence of an opposing Marangoni stress, Eur. Phys. J. E **40**, 9 (2017).

[15] C. Li, H. Xiao, R. Jiang, and X. Ye, Effect of wall slip on vertical film drainage in presence of soluble surfactants, Phys. Fluids **33**, 042113 (2021).

[16] N. Xue, M. Y. Pack, and H. A. Stone, Marangoni-driven film climbing on a draining pre-wetted film, J. Fluid Mech. **886**, A24 (2020).

[17] G. Ginley and C. Radke, Influence of soluble surfactants on the flow of long bubbles through a cylindrical capillary, ACS Symp. Ser. **396**, 480 (1989).

[18] J. Ratulowski and H.-C. Chang, Marangoni effects of trace impurities on the motion of long gas bubbles in capillaries, J. Fluid Mech. **210**, 303 (1990).

[19] C.-W. Park, Influence of soluble surfactants on the motion of a finite bubble in a capillary tube, Phys. Fluids **4**, 2335 (1992).

[20] H. Kim, F. Boulogne, E. Um, I. Jacobi, E. Button, and H. A. Stone, Controlled uniform coating from the interplay of Marangoni flows and surface-adsorbed macromolecules, Phys. Rev. Lett. **116**, 124501 (2016).

[21] X. Xu, J. Luo, and D. Guo, Criterion for reversal of thermal Marangoni flow in drying drops, Langmuir **26**, 1918 (2010).

[22] S. Shiri, S. Sinha, D. A. Baumgartner, and N. J. Cira, Thermal Marangoni flow impacts the shape of single component volatile droplets on thin, completely wetting substrates, Phys. Rev. Lett. **127**, 024502 (2021).

[23] M. Gugliotti, M. S. Baptista, and M. J. Politi, Surface tension gradients induced by temperature: The thermal marangoni effect, J. Chem. Educ. **81**, 824 (2004).

[24] X. Fanton and A. Cazabat, Spreading and instabilities induced by a solutal Marangoni effect, Langmuir **14**, 2554 (1998).

[25] H. Kim, K. Muller, O. Shardt, S. Afkhami, and H. A. Stone, Solutal Marangoni flows of miscible liquids drive transport without surface contamination, Nat. Phys. **13**, 1105 (2017).

[26] J. Ryu, J. Kim, J. Park, and H. Kim, Analysis of vapor-driven solutal Marangoni flows inside a sessile droplet, Int. J. Heat Mass Transfer **164**, 120499 (2021).

[27] T. Still, P. J. Yunker, and A. G. Yodh, Surfactant-induced Marangoni eddies alter the coffee-rings of evaporating colloidal drops, Langmuir **28**, 4984 (2012).

[28] R. T. van Gaalen, H. M. A. Wijshoff, J. G. M. Kuerten, and C. Diddens, Competition between thermal and surfactant-induced Marangoni flow in evaporating sessile droplets, J. Colloid Interface Sci. **622**, 892 (2022).

[29] A. Mizev and A. Trofimenko, Effect of an insoluble surfactant film on the stability of the concentration-driven Marangoni flow, Fluid Dyn. **49**, 26 (2014).

[30] H. Li, Z. Li, X. Tan, X. Wang, S. Huang, Y. Xiang, P. Lv, and H. Duan, Three-dimensional backflow at liquid–gas interface induced by surfactant, J. Fluid Mech. **899**, A8 (2020).

[31] D. Halpern, Y.-C. Li, and H.-H. Wei, Slip-induced suppression of Marangoni film thickening in surfactant-retarded Landau–Levich–Bretherton flows, J. Fluid Mech. **781**, 578 (2015).

[32] E. D. Manev and A. V. Nguyen, Effects of surfactant adsorption and surface forces on thinning and rupture of foam liquid films, Int. J. Miner. Process. **77**, 1 (2005).

[33] M. Winkler, G. Kofod, R. Krastev, S. Stöckle, and M. Abel, Exponentially fast thinning of nanoscale films by turbulent mixing, Phys. Rev. Lett. **110**, 094501 (2013).

[34] I. Ivanov, D. Dimitrov, P. Somasundaran, and R. Jain, Thinning of films with deformable surfaces: Diffusion-controlled surfactant transfer, Chem. Eng. Sci. **40**, 137 (1985).

[35] S. Jin, J. Graebner, G. Kammlott, T. Tiefel, S. Kosinski, L. Chen, and R. Fastnacht, Massive thinning of diamond films by a diffusion process, Appl. Phys. Lett. **60**, 1948 (1992).

[36] R. Krechetnikov and G. Homsy, Experimental study of substrate roughness and surfactant effects on the Landau-Levich law, Phys. Fluids **17**, 102108 (2005).

[37] E. Ruckenstein and R. K. Jain, Spontaneous rupture of thin liquid films, *Wetting Theory* (CRC, Boca Raton, FL, 2018), pp. 588–603.

[38] L. S. H. Chow and H. S. Cheng, The effect of surface roughness on the average film thickness between lubricated rollers, J. Lubr. Technol. **98**, 117 (1976).

[39] M. T. Kreutzer, M. S. Shah, P. Parthiban, and S. A. Khan, Evolution of nonconformal Landau-Levich-Bretherton films of partially wetting liquids, Phys. Rev. Fluids **3**, 014203 (2018).

[40] D. Tabor, The role of surface and intermolecular forces in thin film lubrication, *Tribology Series* (Elsevier, New York, 1981), Vol. 7, pp. 651–682.

[41] J. A. Tallmadge and R. Stella, Some properties of the apparent water paradox in entrainment, AIChE J. **14**, 838 (1968).

[42] M. Rao, F. Lefèvre, S. Khandekar, and J. Bonjour, Understanding transport mechanism of a self-sustained thermally driven oscillating two-phase system in a capillary tube, Int. J. Heat Mass Transfer **65**, 451 (2013).

[43] Y. E. Yu, S. Khodaparast, and H. A. Stone, Separation of particles by size from a suspension using the motion of a confined bubble, Appl. Phys. Lett. **112**, 181604 (2018).

[44] N. J. Alvarez, L. M. Walker, and S. L. Anna, A microtensiometer to probe the effect of radius of curvature on surfactant transport to a spherical interface, Langmuir **26**, 13310 (2010).

[45] D. Halpern and J. Grotberg, Dynamics and transport of a localized soluble surfactant on a thin film, J. Fluid Mech. **237**, 1 (1992).

[46] N. J. Alvarez, L. M. Walker, and S. L. Anna, Diffusion-limited adsorption to a spherical geometry: The impact of curvature and competitive time scales, Phys. Rev. E **82**, 011604 (2010).

[47] P. Pico, L. Kahouadji, S. Shin, J. Chergui, D. Juric, and O. K. Matar, Drop encapsulation and bubble bursting in surfactant-laden flows in capillary channels, Phys. Rev. Fluids **9**, 034001 (2024).

[48] Q. Mao, Q.-J. Yang, D.-X. Wang, and W. Cao, Effect of soluble surfactant on the interface dynamics of a rising droplet, Phys. Fluids **35**, 033602 (2023).

[49] C. R. Constante-Amores, L. Kahouadji, A. Batchvarov, S. Shin, J. Chergui, D. Juric, and O. K. Matar, Dynamics of a surfactant-laden bubble bursting through an interface, J. Fluid Mech. **911**, A57 (2021).

[50] F. M. Menger and S. A. Rizvi, Relationship between surface tension and surface coverage, Langmuir **27**, 13975 (2011).

[51] C. Extrand, Spontaneous draining of liquids from vertically oriented tubes, Langmuir **33**, 12903 (2017).

[52] F. M. White, *Fluid Mechanics* (The McGraw Hill Companies, New York, 2008).

[53] H. Jeffreys, The draining of a vertical plate, Math. Proc. Cambridge Philos. Soc. **26**, 204 (1930).

[54] See Supplemental Material at http://link.aps.org/supplemental/10.1103/PhysRevFluids.9.094005 for videos of the meniscus drainage over various surfactant concentrations.